energy&fuels

Article

pubs.acs.org/EF

Hydrodeoxygenation of Methyl Palmitate over Supported Ni Catalysts for Diesel-like Fuel Production

Hualiang Zuo,[†,‡] Qiying Liu,[†] Tiejun Wang,[†,*] Longlong Ma,[†,*] Qi Zhang,[†] and Qing Zhang[†]

[†]Key Laboratory of Renewable Energy and Gas Hydrate, Guangzhou Institute of Energy Conversion, Chinese Academy of Sciences, Guangzhou 510640, People's Republic of China

[‡]Graduate School of Chinese Academy of Sciences, Beijing 100049, People's Republic of China

ABSTRACT: Catalytic hydrodeoxygenation (HDO) of vegetable oils to renewable alkane-type biofuels has attracted more and more concern in recent years. However, the presently used catalysts were mainly focused on the sulfided CoMo and NiMo catalysts, which inevitably posed sulfur contamination in final products. Therefore, exploring nonsulfured catalyst for this processing is of fundamental importance, but it is still an open challenge. In this paper, we prepared the sulfur free Ni supported on SiO_2, γ-Al_2O_3, SAPO-11, HZSM-5, and HY by incipient wetness impregnation and tested the catalytic performance in HDO of methyl palmitate. Alkanes with long carbon chains were mainly produced with two possibly parallel approaches: hydrogenation of hexadecanal to hexadecanol, followed by dehydration/hydrogenation to C_{16} alkane and decarbonylaton/decarboxylation of hexadecanoic acid to C_{15} alkane. The acidity of catalysts significantly influenced their catalytic performance, and the Ni/SAPO-11 catalysts with weak and medium acidity showed superior properties to the other catalysts due to the synergistic effect of metal Ni and acidic support. The maximum yield of 93% for C_{15+} alkanes was observed over 7 wt % Ni/SAPO-11 under the mild reaction conditions of 493 K and 2 MPa, indicating its promising application in this reaction.

1. INTRODUCTION

Fast development of modern industry and continued depletion of fossil energy entailed significant environment pollution and greenhouse CO_2 emission, which forces researchers worldwide to focus their vision on renewable energy for substituting the present fossil fuels. Of those renewable fuels, biofuel has received significant interest in the past decade because it presents as a unique carbon included fuel that is favorable for transportation.[1,2] Currently, biodiesel produced by transesterification of vegetable oils and methanol is widely used as a renewable fuel.[3−9] However, biodiesel usually suffers from disadvantageous fuel properties such as relatively high freezing point due to the involved oxygen atoms, and limited compatibility with gas engines, low chemical stability, and low caloric value due to the involved oxygen atoms and the unsaturated C−C bonds, as comparing with the present fossil fuels.[10−13] In order to overcome these disadvantages of biodiesel, catalytic hydrodeoxygenation (HDO, the essential removal of oxygen atoms and saturation of unsaturated C−C bonds) of biomass derived fatty acids,[14,15] aliphatic esters[11,16−18] and/or vegetable oils[19−21] for the production of diesel-like hydrocarbon fuels has been intensively investigated in recent years.

The primary HDO catalysts were mainly concentrated on dispersing noble metals Pt,[11] Pd,[14] and transition metals Ni−Mo, Co−Mo, and Ni−W on the supports of γ-Al_2O_3,[16−18] activation carbon,[14] SiO_2,[21] and SBA-15,[15] etc. Noble metals showed high activity and stability, but their extortionate cost limits their essential application on a large scale. On the other hand, the transition metals Ni and Co with promoters of Mo or W were comparable to the noble metals. NiMo/γ-Al_2O_3 and CoMo/γ-Al_2O_3 catalysts were widely used in HDO of vegetable oils for producing high yield of hydrocarbon fuels,[16−18] and the HDO mechanism investigation revealed that HDO of vegetable oils is a multistep reaction with oxygen-containing compounds including aliphatic alcohols and fatty acids as the intermediates.[22,23] Aside from the above-mentioned HDO pathway, decarbonylation and/or decarboxylation also occurred parallel with obtaining the main products of aliphatic chain length hydrocarbons containing one less carbon than the corresponding feedstocks.[15] It is noted that although these modified transition metals showed a highly catalytic performance in this kind of HDO reaction, the introduction of sulfur containing agents is necessary to keep the sulfided state of catalysts during catalyst pretreatment and HDO processing, which inevitably brings about sulfur pollution in the final products. For example, a previous report testified that the maximum molar concentration of heptanethiol in the liquid products was 0.4% with 400 ppm of H_2S addition, during HDO of methyl heptanoate over the sulfided NiMo/γ-Al_2O_3 catalysts.[24] Therefore, exploring nonsulfided metal catalyst for avoiding such drawbacks is of fundamental importance, but it still an open challenge.

It is well-known that the exposed acid/base sites of the catalyst support could also participate in the activation of reactants and play the essential role in governing product distribution. For example, significantly increased cracking C_1−C_4 alkanes, aromatization arenes, and severe carbon deposition were observed with using strong acidic HZSM-5 zeolite as catalyst.[25] Comparatively, over basic MgO, the heavy alkanes with carbon number of more than 35 were mainly manufactured due to C−C coupling of fatty ester intermedi-

Received: January 13, 2012
Revised: May 13, 2012
Published: May 14, 2012

dx.doi.org/10.1021/ef300063b | *Energy Fuels* 2012, 26, 3747−3755

Table 1. HDO of Methyl Palmitate over Supported Ni Catalysts[a]

		products distribution (mol %)											
						C_5–C_{14}		C_{15}		C_{16}			
catalyst	conversion (%)	DME	CO	CO_2	C_1–C_4	i[b]	n[c]	i	n	i	n	C_{16}+	palmitic acid
7 wt % Ni/SiO_2	49.3	0.05	1.43	0.13	7.69	2.37	14.47	0.00	61.00	0.00	5.97	6.92	0.00
7 wt % Ni/γ-Al_2O_3	90.9	1.11	0.80	0.03	2.02	0.00	3.06	0.00	71.71	0.00	16.72	4.08	0.50
7 wt % Ni/SAPO-11	99.8	1.12	0.83	0.01	2.21	0.00	2.60	0.18	47.45	2.89	39.59	3.11	0.00
7 wt % Ni/HZSM-5	99.7	1.00	1.16	0.22	34.56	2.41	5.03	3.26	27.28	5.15	17.32	2.43	0.21
7 wt % Ni/HY	98.5	0.07	0.20	0.11	45.43	7.65	10.56	2.05	18.12	3.64	6.33	4.42	1.46

[a]Reaction conditions: T = 493 K, P = 2.0 MPa, t = 360 min. [b]i: isoalkanes. [c]n: normal alkanes.

ates.[26] Unfortunately, such important support mediated evaluation is still seldom reported in HDO of vegetable oils so far.

In this work, we prepared Ni supported on γ-Al_2O_3, SiO_2, HY, HZSM-5, and silicoaluminophosphate-11 (SAPO-11) catalysts by initial wetness impregnation and compared their catalytic performance in HDO of methyl palmitate (the model compound of vegetable oil) to diesel like fuel. The physicochemical properties of catalysts were characterized by X-ray diffraction (XRD), Brunauer–Emmett–Teller (BET), scanning electron microscopy (SEM), thermogravimetric (TG), NH_3-temperature-programmed desorption (NH_3-TPD), H_2-temperature-programmed reduction (H_2-TPR), and H_2-chemisorption techniques, and the possible HDO reaction pathway was proposed.

2. EXPERIMENTAL SECTION

2.1. Materials. Five kinds of support materials γ-Al_2O_3, SiO_2, and HY (Si/Al = 2.91), HZSM-5 (Si/Al = 38), and SAPO-11 (Si/Al = 0.11 and Al/P = 1) zeolites were commercially purchased from Tianjin Chemical Scientific Co., Ltd. Methyl palmitate (Aladdin, purity > 98%), analytic graded $Ni(NO_3)_2{\cdot}6H_2O$, and cyclohexane were provided by Tianjin Fuyu Fine Chemical Co., Ltd. and used without further purification.

2.2. Catalyst Preparation and Characterization. All the Ni-based catalysts were prepared by impregnating the catalyst support in aqueous solution of $Ni(NO_3)_2{\cdot}6H_2O$ with the desired Ni loading. The resultant suspension was stirred for 10 h at ambient temperature, followed by evaporating excess water at 353 K. The solids remained were dried at 393 K and calcined at 823 K for 3 h in air. The catalysts were reduced at 773 K for 3 h under 5 vol. % H_2/N_2 flow before use.

XRD patterns of the catalysts were obtained with using x'pert PRO MPD diffract meter (PANalytical) operated at 40 KV and 40 mA with a Cu K_α (λ = 0.15406 nm) radiation. The catalysts were reduced at 773 K for 3 h under 5 vol. % H_2/N_2 flow before measurement. SEM images were recorded using S-4800 instrument operated at 10 kV. The samples were placed on a conductive carbon tape adhered to an aluminum sample holder. BET surface area and pore size distribution were determined by N_2 isothermal adsorption–desorption behavior at 77 K using a Micrometrics ASAP-2010 automated system. NH_3-TPD experiments were carried out in a homemade instrument equipped with a thermal conductivity detector (TCD). For each run, 100 mg catalyst reduced at 773 K under 5 vol. % H_2/N_2 flow was packed into the U-type quartz tube reactor and pretreated in a flow of nitrogen (30 mL/min) at 873 K for 30 min, and then, the sample was cooled to 393 K for absorbing ammonia until the saturated state was obtained. The physically adsorbed ammonia was removed by purging helium at the same temperature and the NH_3-TPD profile was recorded by programming the temperature from 393 to 873 K, ramping at 10 K/min. H_2-TPR measurements were carried out in the same instrument. 100 mg catalyst was pretreated in a flow of nitrogen (30 mL/min) at 623 K for 30 min, followed by cooling to room temperature. The catalyst was heated from room temperature to 1173 K with the rate of 10 K/min under a flow of 5 vol. % H_2/N_2 (30 mL/min). Hydrogen consumption was monitored by the TCD signal change of the effluent gas stream. TG analyses of the spent catalysts were implemented on a NETZSCH-STA 409PC DSC-SP thermal analyzer by increasing the temperature from 313 to 1073 K at 10 K/min under an air flow rate of 30 mL/min. The H_2-chemisorption instrument was tested with using a Quantachrome-ASIQACIV200-2 automated gas sorption analyzer. The catalyst was reduced at 773 K for 3 h under hydrogen atmosphere. To clean the catalyst surface, the samples were further heated to 823 K under nitrogen, kept at this temperature for 30 min, and then cooled to 323 K for the H_2-chemisorption test.

2.3. Catalytic Performance. HDO of methyl palmitate was carried out in a 100 mL semibatch stainless autoclave furnished with a mechanical stirrer and a condensing tube cooled by flowing ice-cooled water at export. In a typical reaction, 1.0 g freshly reduced catalyst and 30.0 g methyl palmitate were loaded in the autoclave. After removing air in the reactor with argon flushing, H_2 was introduced and pressurized at 2 MPa by pressure regulating valves. The H_2 flow was controlled at 50 mL/min. The reaction system was then heated to 493 K and maintained at this temperature for 360 min. During the reaction, the stirring speed was maintained at 1000 rpm to prevent external mass transfer limitation,[27] and the gas products were collected at every 30 min. After reaction, the reaction system was cooled to ambient temperature, and the liquid products were collected for further analysis.

2.4. Product Analysis. C_1–C_4 hydrocarbons and dimethyl ester (DME) were analyzed by a GC 9800 chromatography equipped with a flame ionization detector (FID) and a packed column (Porapak-Q column, 3 m × 3 mm) by using nitrogen as carrier gas, and CO, CO_2, and CH_4 was analyzed by another GC 9800 equipped with a TCD and a packed column (TDX-01 column, 3 m × 3 mm) with using helium as carrier gas. All of the gas products were quantified by external standard method with using the peak area of CH_4 as correlation.

The liquid products collected were diluted with cyclohexane, identified by GC-MS measurement, and quantified by an Agilent Tecnologies 4890 gas chromatography equipped with a capillary column (DB-1701, 60 m × 0.25 mm ×0.25 μm) and FID by using n-nonadecane as the internal standard.

Conversion of methyl palmitate (X_A) and selectivity of product i (S_i) were defined as

$$X_A\ (\%) = \frac{w_0 - w_1}{w_0} \times 100$$

$$S_i\ (\text{mol}\ \%) = \frac{n_i \times a_i}{\sum_1^i n_i \times a_i} \times 100$$

Here, w_0 refers to the initial weight of methyl palmitate, and w_1 is the weight of final methyl palmitate after reaction; n_i indicates the moles of product i, and a_i represents the carbon atom number of product i.

3. RESULTS AND DISCUSSION

3.1. HDO of Methyl Palmitate. The catalytic performance of Ni catalysts with different supports was compared in HDO

dx.doi.org/10.1021/ef300063b | Energy Fuels 2012, 26, 3747–3755

Table 2. HDO of Methyl Palmitate over Ni/SAPO-11 Catalysts[a]

		products distribution (mol %)										
						C_5-C_{14}		C_{15}		C_{16}		
catalyst	conversion (%)	DME	CO	CO_2	C_1-C_4	i[b]	n[c]	i	n	i	n	C_{16+}
2 wt % Ni/SAPO-11	60.0	4.38	1.33	0.00	0.84	0.00	1.05	0.00	48.04	0.00	35.26	9.09
5 wt % Ni/SAPO-11	93.0	1.58	1.54	0.00	3.20	0.00	2.35	0.00	48.35	0.00	37.50	0.67
7 wt % Ni/SAPO-11	99.8	1.12	0.83	0.01	2.21	0.00	2.60	0.18	47.45	2.89	39.59	3.11
9 wt % Ni/SAPO-11	99.2	1.30	1.36	0.04	2.88	0.08	2.96	0.18	47.76	3.41	37.26	2.74

[a]Reaction conditions: T = 493 K, P = 2.0 MPa, t = 360 min. [b]i: isoalkanes. [c]n: normal alkanes.

Table 3. HDO of Methyl Palmitate over 7 wt % Ni/SAPO-11 Catalyst at Different Reaction Times[a]

		products distribution (mol %)											
						C_5-C_{14}		C_{15}		C_{16}			
reaction time (min)	conversion (%)	DME	CO	CO_2	C_1-C_4	i[b]	n[c]	i	n	i	n	C_{16+}	palmitic acid
180	48.7	1.38	0.65	0.01	3.39	0.00	0.16	0.01	25.80	0.15	6.26	3.33	58.75
360	99.8	1.12	0.83	0.01	2.21	0.00	2.60	0.18	47.45	2.89	39.59	3.11	0.00

[a]Reaction conditions: T = 493 K, P = 2.0 MPa. [b]i for isoalkanes. [c]n for normal alkanes.

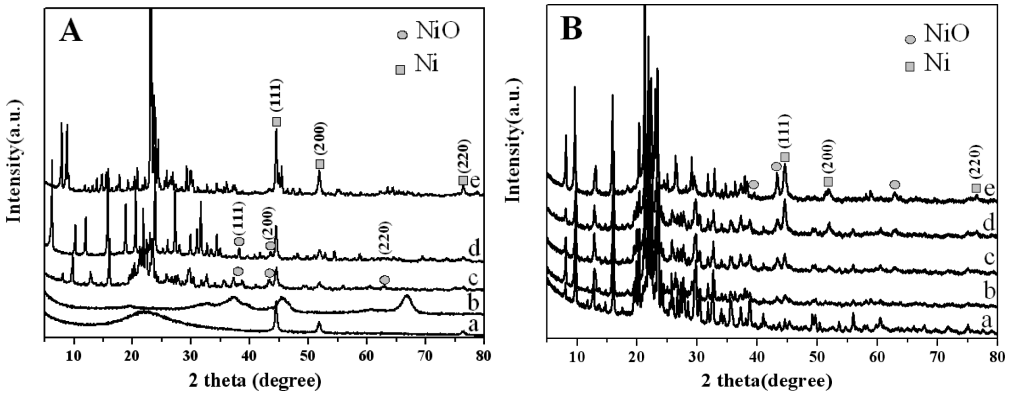

Figure 1. XRD patterns of the supported Ni catalysts (A) for (a) 7 wt % Ni/SiO_2, (b) 7 wt % Ni/γ-Al_2O_3, (c) 7 wt % Ni/SAPO-11, (d) 7 wt % Ni/HY, and (e) 7 wt % Ni/HZSM-5 and the Ni/SAPO-11 catalysts (B) for (a) SAPO-11, (b) 2 wt % Ni/SAPO-11, (c) 5 wt % Ni/SAPO-11, (d) 7 wt % Ni/SAPO-11, and (e) 9 wt % Ni/SAPO-11.

of methyl palmitate under the mild reaction condition of 493 K, 2 MPa of H_2 pressure and 360 min, and the results were listed in Table 1. For all catalysts, the primary products were mainly composed of the gaseous CO, CO_2, dimethyl ether (DME, produced by methanol dehydration) and C_1-C_4 alkanes, the liquid palmitic acid and alkanes with the carbon numbers of more than 5, and the hexadecanal, hexadecanol, and hexadecene intermediates with trace amounts of less than 0.01% (the data are not shown here). Over 7 wt % Ni/SiO_2, the relatively low methyl palmitate conversion and the selectivity to liquid alkane products presented as 49.3% and 90.7%, respectively. Among those products, pentadecane was confirmed as the highest selectivity of 61% with medium amounts of cracking C_1-C_4 and C_5-C_{14}, and coupling C_{16+} (such as heptadecane and octadecane) alkanes. For the 7 wt % Ni/HZSM-5 and 7 wt % Ni/HY catalysts, although the conversions of methyl palmitate were drastically increased to nearly 100%, the target liquid alkanes significantly declined to 63% over 7 wt % Ni/HZSM-5 and 53% over 7 wt % Ni/HY, owing to the obviously incremental selectivities of the unwanted cracking C_1-C_4 alkanes. Comparatively, both 7 wt % Ni/γ-Al_2O_3 and 7 wt % Ni/SAPO-11 presented the high methyl palmitate conversions which were similar to 7 wt % Ni/HZSM-5 and 7 wt % Ni/HY and the high selectivities of liquid alkane products which were resembled to 7 wt % Ni/SiO_2, indicating the superior catalytic performance in HDO of methyl palmitate. For instance, the maximal 99.8% of methyl palmitate conversion and 95.8% of selectivity for the target liquid alkanes were obtained over 7 wt % Ni/SAPO-11. Apart from 7 wt % Ni/γ-Al_2O_3, the Ni based catalysts showed isomerization activity in HDO of methyl palmitate under the given reaction condition, but all the selectivities was less than 2%.

Taking into account that the Ni supported on SAPO-11 showed the best catalytic performance in HDO of methyl palmitate, we further evaluated the properties of Ni/SAPO-11 catalysts with different Ni loadings and the results were summarized in Table 2. As Ni loadings increased from 2 wt % to 7 wt %, conversions of methyl palmitate monotonously increased from 60% to 99.8%, respectively. The selectivities to the liquid alkanes of C_{5+} also slightly increased from 93.4% to 95.8%. Comparatively, as the Ni loading was further increased to 9 wt %, both the conversion of methyl palmitate and the selectivity of C_{5+} alkanes kept almost unchanged. For all Ni/SAPO-11 catalysts, the total selectivities of 83−90% for C_{15} and C_{16} alkanes observed with the relatively low C_{15}/C_{16} ratios and the cracking products were controlled at very low levels.

dx.doi.org/10.1021/ef300063b | Energy Fuels 2012, 26, 3747−3755

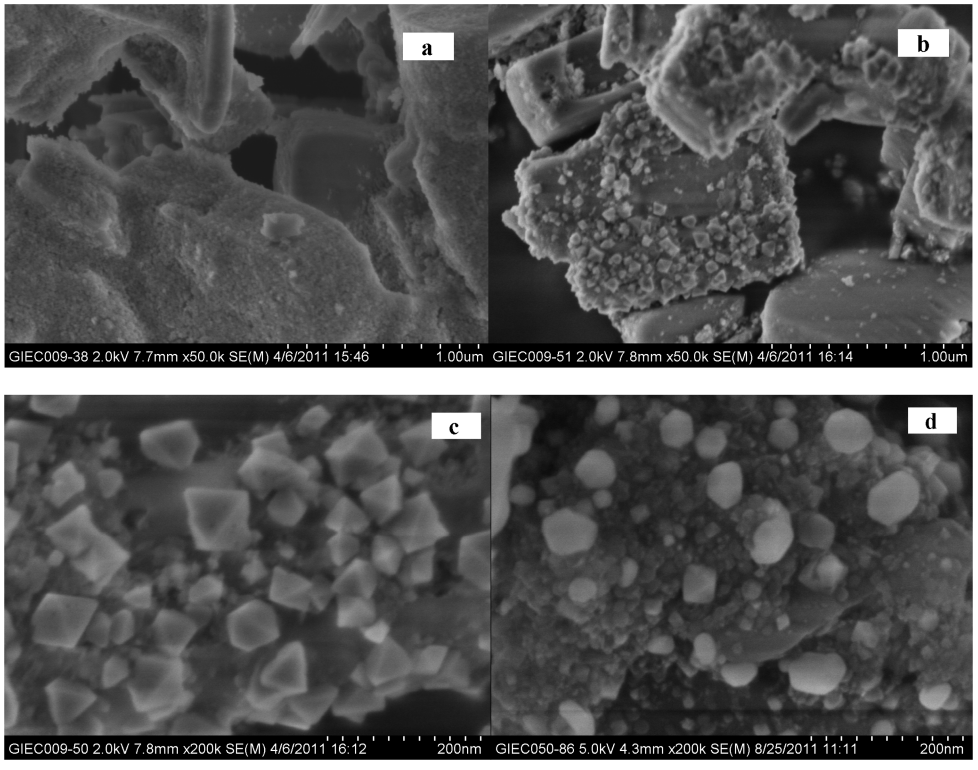

Figure 2. SEM images of the Ni/SAPO-11 catalysts for (a) SAPO-11, (b) 7 wt % Ni/SAPO-11at low magnification and (c) at enlarged magnification, and (d) 7 wt % Ni/SAPO-11 after HDO of methyl palmitate.

Additionally, the selectivities to isoalkanes slightly increased as the Ni loadings increased from 2 wt % to 7 wt %.

The influence of reaction time on the catalytic performance of 7 wt % Ni/SAPO-11 catalyst was shown in Table 3. As reaction time increased, the conversion of methyl palmitate rose significantly and 99.8% of conversion was obtained at 360 min, indicating that methyl palmitate was nearly completely transformed. The reaction time also significantly influenced the production selectivities in HDO of methyl palmitate. At the reaction time of 180 min, the percentages of C_{5+} liquid alkanes and palmitic acid were 25.7% and 58.75%, respectively. When the reaction time was extended to 360 min, none of palmitic acid was detected and the selectivity to the liquid alkanes drastically raised to 95.8%, showing that palmitic acid act as an intermediate and convert into the downstream alkanes during this HDO process. This is well consistent with the previous reports.[22,23] It is noted that CH_4, which is produced by the hydrogenolysis of methyl palmitate and/or the hydrogenation of the primary CO/CO_2 and methanol, was detected as the percentages of more than 90% in the gas hydrocarbon products independent of the reaction time (the data are not shown here).

3.1. Catalyst Characterization. The XRD patterns of the 7 wt % Ni based catalysts with different supports were shown in Figure 1A. The characteristic diffractions associated to the supports of γ-Al_2O_3, SAPO-11, HZSM-5 and HY were presented, indicating that the structures of the employed supports could be largely kept as 7 wt % Ni was impregnated and calcined. Over 7 wt % Ni/SAPO-11, 7 wt % Ni/HZSM-5, and 7 wt % Ni/HY, the characteristic diffraction peaks were clearly observed at 2θ = 44.5°, 51.8°, and 76.4°, corresponding to the (111), (200), and (220) crystallographic planes of face-centered cubic Ni phase, respectively. This demonstrated that only small amounts of Ni could be accommodated in the micropores of SAPO-11, HZSM-5, and HY, the remaining ones aggregating on the external surface of the supports to form particles. Although amorphous SiO_2 generally shows the large surface area, pore sizes, and volume, the Ni phase was also observed as the obvious diffractions, which is possibly due to the weak interactions between the Ni species and SiO_2 surface and leads to significant aggregation in the pore wall of SiO_2. On the other hand, no characteristic diffractions relative to Ni were observed over 7 wt % Ni/γ-Al_2O_3, indicating that the Ni species can be highly dispersed on the surface of γ-Al_2O_3, with their sizes below the detective limitation of the XRD instrument. In addition, characteristic diffraction peaks of NiO (2θ = 37.3°, 43.2°, and 62.8°) were observed with low intensities over 7 wt % Ni/SAPO-11, 7 wt % Ni/HZSM-5, and 7 wt % Ni/HY, which indicates that the supported Ni^{2+} species could not be fully reduced to the metallic state under the given pretreatment condition due to the strong interactions of partial Ni^{2+} species and the supports.

Figure 1B showed the XRD patterns of Ni/SAPO-11 catalysts with different Ni loadings. Diffractive peaks of SAPO-11 could be seen in all diffraction profiles, indicating that the structure of SAPO-11 was largely retained after impregnation and calcination. When the Ni loadings were no more than 2 wt %, the absence of the characteristic diffraction peaks relative to Ni phase indicated the high dispersion of Ni species on SAPO-11 surface, possibly due to some of Ni species being diffused into the microchannels of SAPO-11. As the Ni loadings increased to 5 wt % and above, the diffractions corresponding to NiO and Ni crystallographic phase occurred and their intensities raised with increasing the Ni loadings, which demonstrated that the excessive amounts of Ni deposited

dx.doi.org/10.1021/ef300063b | Energy Fuels 2012, 26, 3747−3755

on the external surface of SAPO-11 and agglomerated into larger particles.

Figure 2 showed the SEM images of the pristine SAPO-11, and the fresh and spent 7 wt % Ni/SAPO-11 catalysts. The pure SAPO-11 presented as a relatively smooth surface with the size of several micrometers. For the fresh 7 wt % Ni/SAPO-11, the support sizes kept almost unchanged and the sizes of the NiO particles were 30−100 nm. The SEM image with a larger magnification (Figure 2c) showed that the NiO particles exclusively presented as the sharp-edged octahedral shape with one side attached to the surface of support and the others exposed to the air. The SEM image of the spent 7 wt % Ni/SAPO-11 was shown in Figure 2d. Despite reduction to the metallic state by H_2 and survival from HDO of methyl palmitate, the Ni particles presented as nonaggregation and its original octahedrons transferred to the spheres with the sizes of 20−80 nm, showing the stability of this catalyst in HDO of methyl palmitate.

Table 4 shows the textural properties and H_2-chemisorption of Ni based catalysts with different supports. The catalyst 7 wt % Ni/HY had the largest surface area, with the external surface of 120.7 m^2/g, indicating that its surface area was mainly contributed by the internal micropores of HY. This was similar to 7 wt % Ni/HZSM-5 catalyst, which possessed the total and external surface area of 173.3 m^2/g and 85.6 m^2/g, respectively. For the 7 wt % Ni/SAPO-11 catalyst, the surface area was 33.5 m^2/g with the external surface area of 33.0 m^2/g, which is possibly due to the supported Ni particles blocking the micropores of SAPO-11 and creating the external surface of 7 wt % Ni/SAPO-11 by Ni particles themselves. Both 7 wt % Ni/SiO_2 and 7 wt % Ni/γ-Al_2O_3 presented large surface areas, pore sizes, and volumes, which is ascribed to the fact that the larger pore sizes and volumes of SiO_2 and γ-Al_2O_3 could accommodate enough Ni particles and no pore blockage occurred. To estimate the dispersions of Ni particles and their sizes, H_2-chemisorption experiments were implemented, and the results were listed in Table 4. Dependent on the support used, the dispersion of Ni particles were 5.1%, 3.8%, and 3.0% and the Ni particle sizes were estimated as 20 nm, 27 nm, and 34 nm over HZSM-5, SiO_2, and SAPO-11, respectively, according to the previous calculation.[28] The Ni particle sizes determined by H_2-chemisorption are well consistent with the SEM results (Figure 2d). For supported Ni catalysts, the dispersion of Ni particles is dependent on the textual and surface properties of supports, and those with large surface areas, pore sizes, and volumes, and strong interactions with Ni^{2+} species facilitated dispersing Ni particles and obtaining the smaller Ni particle sizes. Thus, it is rational that 7 wt % Ni/HZSM-5 and 7 wt % Ni/SiO_2 presented relatively higher Ni dispersions than 7 wt % Ni/SAPO-11.

Table 4. Textural Properties and H_2-Chemisorption of Ni-Based Catalysts with Different Supports

catalyst	S_{BET}[a] (m^2/g)	S_{ex}[b] (m^2/g)	V_p[c] (cm^3/g)	D[d] (%)	d[e] (nm)
7 wt % Ni/SiO_2	133.0		1.97	3.8	27
7 wt % Ni/γ-Al_2O_3	144.1		0.97		
7 wt % Ni/SAPO-11	33.5	33.0	0.08	3.0	34
7 wt % Ni/HZSM-5	173.3	85.6	0.13	5.1	20
7 wt % Ni/HY	616.9	120.7	0.21		

[a]Surface area, calculated by BET method. [b]External surface, calculated from desorption branch by BJH method. [c]Mesoporous volume, calculated from desorption branch by BJH method. [d]D = Ni Dispersion. [e]d = diameter of Ni particle.

Textural properties of Ni/SAPO-11 catalysts were shown in Table 5. The original SAPO-11 presented the total surface area of 86 m^2/g with the minor partition of external surface of 30 m^2/g (created by SAPO-11 particles), which reflected the essential contribution of micropores in surface area of SAPO-11. As Ni was loaded and increased, the total surfaces of the Ni/SAPO-11 catalysts significantly dropped and stabilized at about 33 m^2/g, with the exclusively external surface remaining. On the other hand, the mesoporous volumes (Table 5) and the pore size distributions (Figure 3) of the Ni/SAPO-11 samples gradually declined from 0.096 cm^3/g and 10 nm for the pristine SAPO-11 to 0.078 cm^3/g and 8 nm for 9 wt % Ni/SAPO-11, respectively. SAPO-11, which possesses one-dimensional micropore size of elliptical 0.39 nm ×0.63 nm with a 10-member ring, was first synthesized by substituting Si for P or Al and P in the parent aluminophosphate framework in 1984.[29] It is more likely that such small pore sizes of SAPO-11 could not afford enough space to accommodate the Ni species, even at the low Ni loading of 2 wt %, which inevitably leads to part of Ni species locating on the pore mouth and blocks the microchannels, inducing a significant decrease of microporous surface. As Ni loadings increased, the excessive Ni stacks on the external surface of the support and grows into larger particles, resulting in the mesoporous volumes and pore sizes of the Ni/SAPO-11 catalysts decreasing gradually.

Table 5. Textural Properties of Ni/SAPO-11 Catalysts

catalyst	S_{BET}[a] (m^2/g)	S_{ex}[b] (m^2/g)	V_p[c] (cm^3/g)
SAPO-11	85.6	29.7	0.096
2 wt % NiSAPO-11	33.5	31.6	0.086
5 wt % NiSAPO-11	33.3	32.5	0.081
7 wt % NiSAPO-11	33.5	33.0	0.083
9 wt % NiSAPO-11	33.0	28.6	0.078

[a]Surface area, calculated by BET method. [b]External surface, calculated from desorption branch by BJH method. [c]Mesoporous volume, calculated from desorption branch by BJH method.

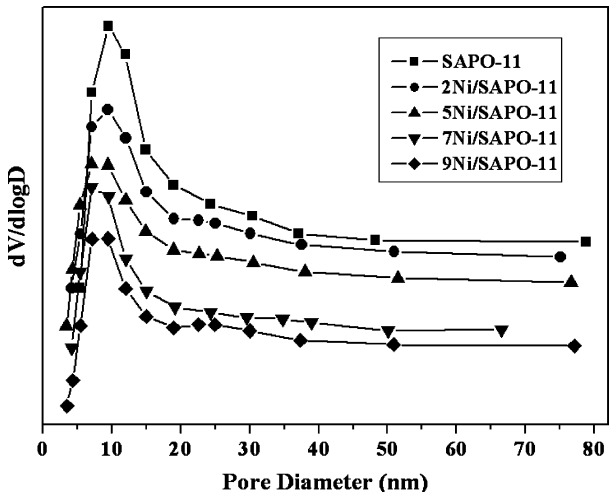

Figure 3. Pore size distribution of Ni/SAPO-11 catalysts with different Ni loadings.

dx.doi.org/10.1021/ef300063b | Energy Fuels 2012, 26, 3747−3755

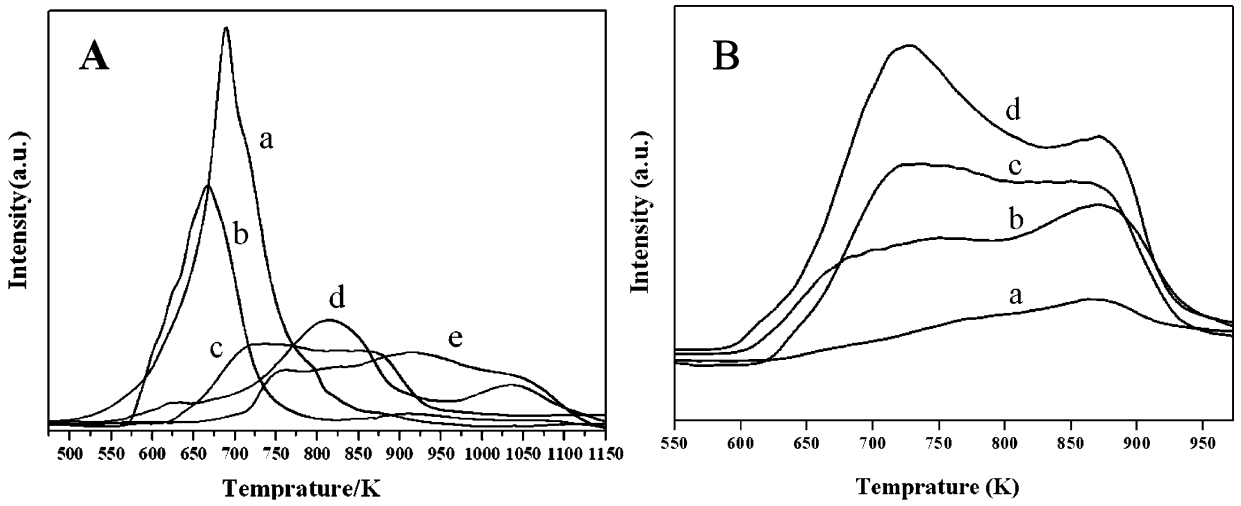

Figure 4. H_2-TPR profiles for (A) the supported Ni catalysts, (a) 7 wt % Ni/HZSM-5, (b) 7 wt % Ni/SiO_2, (c) 7 wt % Ni/SAPO-11, (d) 7 wt % Ni/HY, and (e) 7 wt % Ni/γ-Al_2O_3 and (B) the Ni/SAPO-11 catalysts, (a) 2 wt % Ni/SAPO-11, (b) 5 wt % Ni/SAPO-11, (c) 7 wt % Ni/SAPO-11, and (d) 9 wt % Ni/SAPO-11.

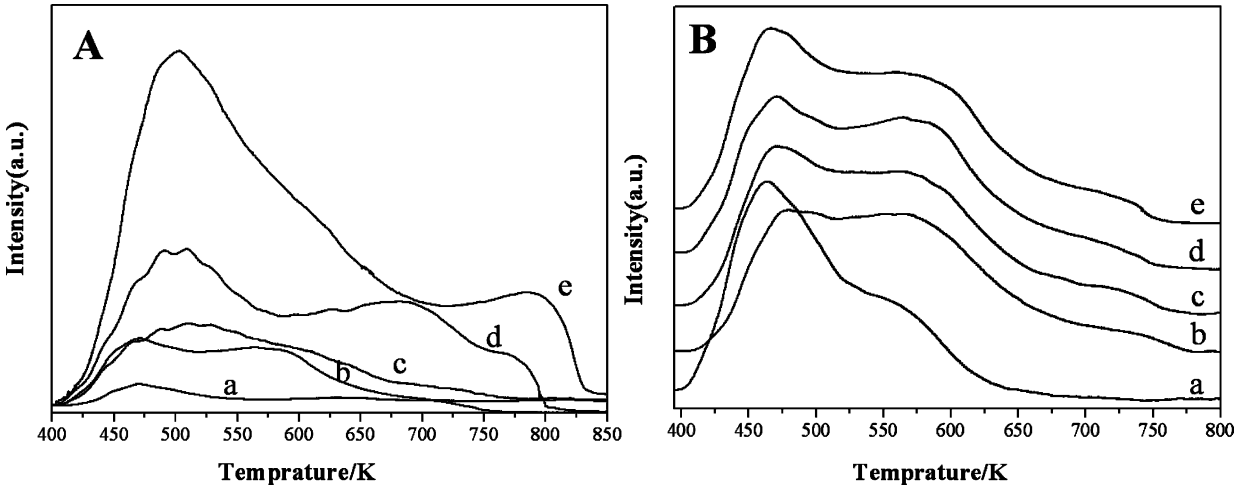

Figure 5. NH_3-TPD profiles for (A) the supported Ni catalysts, (a) 7 wt % Ni/SiO_2, (b) 7 wt % Ni/SAPO-11, (c) 7 wt % Ni/γ-Al_2O_3, (d) 7 wt % Ni/HZSM-5, and (e) 7 wt % Ni/HY and (B) the Ni/SAPO-11 catalysts, (a) SAPO-11, (b) 2 wt % Ni/SAPO-11, (c) 5 wt % Ni/SAPO-11, (d) 7 wt % Ni/SAPO-11, and (e) 9 wt % Ni/SAPO-11.

Figure 4A showed the H_2-TPR profiles of the Ni based catalysts with different supports. Over 7 wt % Ni/HZSM-5 and 7 wt % Ni/SiO_2, the single H_2-consumption peaks were observed at 690 K for HZSM-5 and at 665 K for SiO_2, indicating the reduction of bulky NiO due to the weak interaction between Ni^{2+} and supports.[30] For 7 wt % Ni/SAPO-11, two reduction peaks presented at 725 and 870 K, showing that two distinct Ni^{2+} species of easily reduced and relatively hardly reduced simultaneously existed on the surface of SAPO-11. Comparatively, 7 wt % Ni/γ-Al_2O_3 presented three superimposed reduction peaks at the low temperature of 760 K, the medium temperature of 920 K, and the high temperature of 1050 K, which is probably responsible for the reduction of the bulk or free NiO phase; the Ni^{2+} species directly bonded to γ-Al_2O_3 via bridged oxygen atoms and the incorporated Ni^{2+} of spinel $NiAl_2O_4$, respectively.[31] On the other hand, 7 wt % Ni/HY showed the similar three reduction peaks but with the peaks at the low and the medium temperature shifting to 625 and 815 K, respectively, and keeping the peak at the high temperature almost unchanged. In terms of the previous report, the peak at the medium temperature is attributed to the reduction of the Ni^{2+} localized in the supercage and/or sodalite cavities, while the peak at the high temperature is due to the reduction of the Ni^{2+} localized in the hexagonal cavities.[32]

The H_2-TPR profiles of the Ni/SAPO-11 catalysts were presented in Figure 4B. For 2 wt % Ni/SAPO-11, the reduction peak appeared mainly at 870 K with the a broad shoulder centered at 775 K, indicating that two different kinds of Ni^{2+} species, which are reduced at low and high temperature by H_2, respectively, existed on such catalyst surface. With the Ni loading increased, the peak areas relative to high temperature of the Ni/SAPO-11 catalysts increased gradually accompanied with those at low temperatures significantly rising and shifting to the declined temperatures, making the catalyst surface mainly comprise the easily reduced Ni^{2+} species at the Ni loadings of more than 7 wt %. Previous reports revealed that, for immobilizing Ni on an oxide support, a bimodal nature of oxidic Ni species fixed to support presented and consisted of the free NiO particles and the interactional Ni^{2+} species covalently combined with support by bridge oxygen atoms,

dx.doi.org/10.1021/ef300063b | Energy Fuels 2012, 26, 3747−3755

Scheme 1. Proposed Reaction Pathway in HDO of Methyl Palmitate

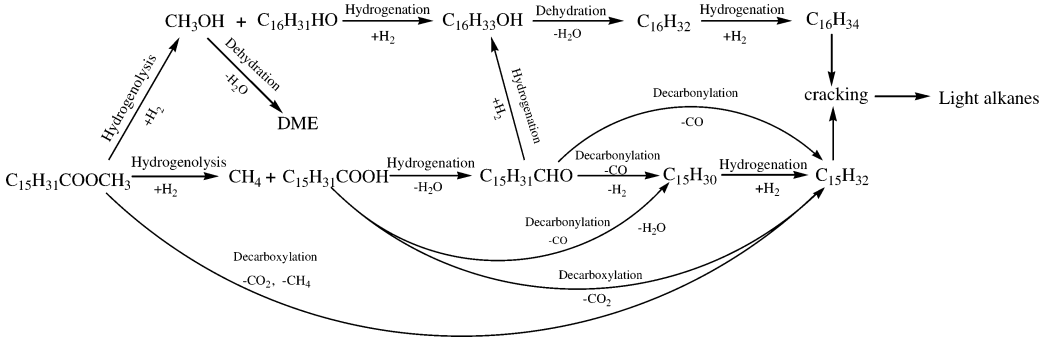

leading to the latter Ni^{2+} species reduced at higher temperatures.[31,33] In the present cases, the Ni^{2+} species at low loadings could highly disperse on SAPO-11 surface, with most directly combining to the support and hardly reduced by H_2, bringing about their reduction peaks located at higher temperatures, while more bulky NiO particles produced at the incremental Ni loadings, thus shifting the corresponding reduction peaks to the declined temperatures. These Ni^{2+} species with strongly interacted with SAPO-11 act as a binding to fix the metallic Ni particles from coalescence during HDO of methyl palmitate.

Figure 5A showed the NH_3-TPD profiles of the Ni based catalysts with different supports. In the spectra of 7 wt % Ni/SiO_2 catalyst, only a small hump centered at 470 K was observed, showing that this catalyst presented the very weak acidity and small acidic sites. For 7 wt % Ni/γ-Al_2O_3, two broad NH_3 desorption peaks appeared at about 515 and 607 K, assigning to the weak and medium acidic sites, respectively, which was well consistent with the previous report.[34] For 7 wt % Ni/SAPO-11, the NH_3 desorption peak location of low temperature was at 470 K with a broad shoulder centered at 586 K, demonstrating that both the weak and the medium acidic sites presented simultaneously on this catalyst surface. According to the previous report, these weak acidic sites were possibly characterized as Brønsted or Lewis type, while the medium ones at relatively high temperature corresponded to the Brønsted sites, which originated from incorporation of Si into the framework of $AlPO_4$ for replacing P.[35] Using zeolite HY as the support, the NH_3 desorption peak was mainly presented at 502 K with an additional small hump at about 795 K, evidencing that both the weak and the strong acidic sites appeared with the weak acidity as the majority. It is highly possible that this large amount of acidic sites is attributed to the high Al content in HY zeolite (Si/Al = 2.91). As for 7 wt % Ni/HZSM-5, three distinct NH_3 desorption peaks corresponding to weak and strong acidic sites appeared at 500, 690, and 775 K, respectively, and the peak area of strong acidity is comparable to that of the weak one.

The NH_3-TPD profiles of Ni/SAPO-11 catalysts with different Ni loadings were shown in Figure 5B. As compared to the pristine SAPO-11, the total acidic amounts of the Ni/SAPO-11 catalysts decreased gradually, while with the medium acidic sites significantly increased. This drop of total acidic sites is possibly ascribed to the inaccessibility of SAPO-11 microchannels, which are impeded by Ni impregnation. On the other hand, those increased medium acidic sites over the Ni/SAPO-11 catalysts seem to be generated by the supported Ni particles, as indicated by the previous report.[36]

3.3. Discussion. HDO of vegetable oils usually presented a complicated reaction network of parallel and/or consecutive hydrogenation, decarboxylation/decarbonylation, dehydration, cracking, and carbon deposition, which involved the oxygenates such as methanol, hexadecanoic acid, hexadecanal, and hexadecanol as the intermediates and CO_2, CO, and alkanes as the final products.[18,23,37,38] As shown in Scheme 1, alkanes with long chains are mainly produced by the following two distinct approaches. The hexacanal intermediate is produced by hydrogenolysis of methyl palmitate, and further hydrogenated to C_{16} alkane through hexadecanol and dexadecene (dehydration of hexadecanol). Due to the very fast transformation for the aldehyde hydrogenation, the alcohol dehydration and the corresponding hexadecene hydrogenation, these intermediates were detected as trace amounts in the final products (all the contents were less than 0.01%). On the other hand, hexadecanoic acid intermediate, which is produced by an alternative hydrogenolysis of methyl palmitate, could be decarbonylized/decarboxylized to C_{15} alkane with CO/CO_2 as the byproducts or directly hydrogenated to C_{16} alkane via hexacanal, hexacanol, and hexadecene as the sequential intermediates. Both C_{15} and C_{16} alkane could be cracked into the light alkanes over acidic catalysts. Considering H_2O formed from methanol and hexadecanol dehydration, hexadecanoic acid intermediate could be also produced by methyl palmitate hydrolysis. It is noted that although the decarbonylation/decarboxylation approach is proposed based on hexadecanoic aicd intermediate, the similar transformation might also occur over methyl palmitate feedstock because of their similar molecular structure.

HDO of methyl palmitate (Table 1) showed that the acidity of the catalysts significantly promoted conversion of methyl palmitate and tailored the product distribution. With aiming to yield higher liquid alkanes, the catalysts (such as γ-Al_2O_3 and SAPO-11) with relatively small acidic sites and simultaneously presented weak and medium acidity are appropriate. For these bifunctional catalysts, the acidity promoted effect could be supposed that the electrophilic acidic sites of catalyst surface activate the carbonyl and/or bridge oxygen atoms of methyl palmitate, weakening the acyl and/or ether bond, which is favorable to be attacked by the over spilled H atoms activated from the adjacent Ni.[39] This results in the formation of 1-hexadecanal and methanol by the acyl bond activation and/or hexadecanoic acid and methane by the ether bond activation, both of which are followed by hydrodeoxygenation and/or decarbonylation/decarboxylation to the final C_{15} and C_{16} alkanes. Furthermore, acidic function of catalysts could also mediate product selectivity via controlling competitive hydrogenation and decarbonylation/decarboxylation during HDO of methyl palmitate. Over 7 wt % Ni/SiO_2 with weak acidity, the abundant C_{15} alkane and the high ratio of C_{15} to C_{16} mean that

dx.doi.org/10.1021/ef300063b | Energy Fuels 2012, 26, 3747−3755

HDO of methyl palmitate basically proceed as the manner of decarbonylation/decarboxylation due to the dominant metal Ni effect.[40]

As medium acidity introduced, the selectivities of C_{16} alkane significantly enhanced due to its promotion effect via hydrogenation. The comparable contents for C_{15} and C_{16} alkanes indicate the balance of the acidity and metal of Ni/SAPO-11 catalysts employed (Table 2). However, the strong acidity posed the significantly incremental selectivities of the gaseous C_1−C_4 alkanes at the expense of those for C_{15} and C_{16} alkanes, indicating the severe cracking of the produced long chain alkanes. The medium acidity of the catalysts could also suppress carbon deposition as comparing to the strong ones. As shown in Figure 6, the carbon deposition over the spent 7 wt % Ni/SAPO-11 was 9%, while the value comparatively increased to 13% as the spent 7 wt % Ni/HZSM-5 was used. For all Ni based catalysts, the long chain alkanes with the carbon number of more than 16 (for example, heptadecane and octadecane) are possibly produced by coupling of long chain olefins dehydrated from the corresponding fatty alcohol and small cracking hydrocarbons,[11,41] although the detailed formation mechanism needs to be further investigated.

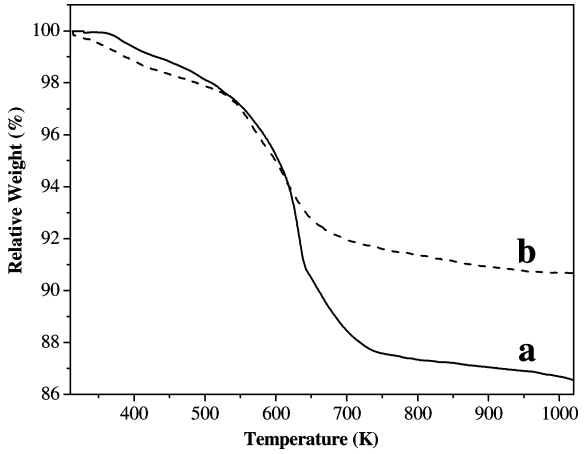

Figure 6. TG curves of the used catalysts for (a) 7 wt % Ni/HZSM-5 and (b) 7 wt % Ni/SAPO-11.

4. CONCLUSIONS

Supported Ni catalysts on HY, HZSM-5, SiO_2, γ-Al_2O_3, and SAPO-11 were prepared by incipient wetness impregnation. γ-Al_2O_3 with large surface areas and pore sizes could highly disperse Ni particles via strong interactions. By contrast, the loaded Ni exclusively agglomerated into particles with sizes of several tens of nanometers over the external surface of SAPO-11, HZSM-5, and HY with the microchannels. The acidic sites and strength of the catalysts follows the order: 7 wt % Ni/SiO_2 < 7 wt % Ni/SAPO-11 < 7 wt % Ni/γ-Al_2O_3 < 7 wt % Ni/HZSM-5 < 7 wt % Ni/HY. In HDO of methyl palmitate, Ni/SAPO-11 with weak and medium acidity showed the superior catalytic performance to the other catalysts due to the synergistic effect that the acidic sites of SAPO-11 promoted activation of methyl palmitate, followed by attacking of H atoms spilled over from metal Ni sites nearby, which obtained higher yield for the alkanes in diesel range. The maxim diesel-like alkane yield of 93% was observed over 7 wt % Ni/SAPO-11 under mild reaction condition, showing its promising catalytic application in this reaction.

AUTHOR INFORMATION

Corresponding Author

*Tel: +86-20-87057751. Fax: +86-20-87057737. E-mail: wangtj@ms.giec.ac.cn. Tel: +86-20-87057673. Fax: +86-20-87057673. E-mail: mall@ms.giec.ac.cn.

Notes

The authors declare that no competing interests exist.

ACKNOWLEDGMENTS

The authors gratefully acknowledge the financial support from the National Basic Research Program of China (2012CB215304), the Natural Science Foundation of China (51161140331), the international co-operation project of the Ministry of Science and Technology of China (2012DFA61080), and the EU-China Cooperation for Liquid Fuels from Biomass Pyrolysis (246772).

REFERENCES

(1) Sharma, Y. C.; Singh, B.; Upadhyay, S. N. *Fuel* **2008**, *87*, 2355−2373.
(2) Agarwal, A. K. *Prog. Energy Combust. Sci.* **2007**, *33*, 233−271.
(3) Marchetti, J. M.; Miguel, V. U.; Errazu, A. F. *Renewable Sustainable Energy Rev.* **2007**, *11*, 1300−1311.
(4) Lotero, E.; Liu, Y.; Lopez, D. E.; Suwannakarn, K.; Bruce, D. A.; Goodwin, J. G. *Ind. Eng. Chem. Res.* **2005**, *44*, 5353−5363.
(5) Demirbas, A. *Energy Convers. Manage.* **2003**, *44*, 2093−2109.
(6) Barakos, N.; Pasias, S.; Papayannakos, N. *Bioresour. Technol.* **2008**, *99*, 5037−5042.
(7) Alonso, D. M.; Mariscal, R.; Moreno-Tost, R.; Poves, M. D. Z.; Granados, M. L. *Catal. Commun.* **2007**, *8*, 2074.
(8) Saka, S.; Kusdiana, D. *Fuel* **2001**, *80*, 225−231.
(9) Terigar, B. G.; Balasubramanian, S.; Lima, M.; Boldor, D. *Energy Fuels* **2010**, *24*, 6609−6615.
(10) Lotero, E.; Liu, Y.; Lopez, D. E.; Suwannakarn, K.; Bruce, D. A.; Goodwin, J. G. *Ind. Eng. Chem. Res.* **2005**, *44*, 5353−5363.
(11) Do, P. T.; Chiappero, M.; Lobban, L. L.; Resasco, D. E. *Catal. Lett.* **2009**, *130*, 9−18.
(12) Donnis, B.; Egeberg, R.; Blom, P.; Knudsen, K. *Top. Catal.* **2009**, *52*, 229.
(13) Senol, O. I.; Ryymin, E. M.; Viljava, T. R.; Krause, A. O. I. *J. Mol. Catal. A: Chem.* **2007**, *277*, 107−112.
(14) Lestari, S.; Simakova, I.; Tokarev, A.; Maki-Arvela, P.; Eranen, K.; Murzin, D. Y. *Catal. Lett.* **2008**, *122*, 247−251.
(15) Lestari, S.; Maki-Arvela, P.; Eranen, K.; Beltramini, J.; Lu, G.; Murzin, D. Y. *Catal. Lett.* **2010**, *134*, 250−257.
(16) Senol, O. I.; Viljava, T. R.; Krause, A. *Catal. Today* **2005**, *106*, 186−189.
(17) Senol, O. I.; Viljava, T. R.; Krause, A. *Catal. Today* **2005**, *100*, 331−335.
(18) Senol, O. I.; Ryymin, E. M.; Viljava, T. R.; Krause, A. *J. Mol. Catal. A: Chem.* **2007**, *268*, 1−8.
(19) Murata, K.; Liu, Y.; Inaba, M.; Takahara, I. *Energy Fuels* **2010**, *24*, 2404−2409.
(20) Morgan, T.; Grubb, D.; Santillan-Jimenez, E.; Crocker, M. *Top. Catal.* **2010**, *53*, 820−829.
(21) Chiappero, M.; Do, P.; Crossley, S.; Lobban, L. L.; Resasco, D. E. *Fuel* **2011**, *90*, 1155−1165.
(22) Senol, O. I.; Viljava, T. R.; Krause, A. *Appl. Catal., A* **2007**, *326*, 236−244.
(23) Ryymin, E. M.; Honkela, M. L.; Viljava, T. R.; Krause, A. *Appl. Catal., A* **2009**, *358*, 42−48.
(24) Turpeinen, E. M. Doctoral dissertation, Aalto University, 2011, p 35.
(25) Sharma, R. K.; Bakhshi, N. N. *Can. J. Chem. Eng.* **1991**, *69*, 1071−1081.

(26) Snare, M.; Kubickova, I.; Maki-Arvela, P.; Eranen, K.; Murzin, D. Y. *Ind. Eng. Chem. Res.* **2006**, *45*, 5708−5715.
(27) Shi, N.; Liu, Q. Y.; Jiang, T.; Wang, T. J.; Ma, L. L.; Zhang, Q.; Zhang, X. H. *Catal. Commun.* **2012**, *20*, 80−84.
(28) Takai, T.; Yeno, A.; Kotera, Y. *Bull. Chem. Soc. Jpn.* **1983**, *56*, 2941−2944.
(29) Lok, B. M.; Messina, C. A.; Patton, R. L.; Gajek, R. T.; Cannan, T. R.; Flanigen, E. M. U.S. Patent No. 4440871, 1984.
(30) Venugopal, A.; Kumar, S. N.; Ashok, J.; Prasad, D. H.; Kumari, V. D.; Prasad, K. B. S.; Subrahmanyam, M. *Int. J. Hydrogen Energy* **2007**, *32*, 1782−1788.
(31) Rynkowski, J. M.; Paryjczak, T.; Lenik, M. *Appl. Catal., A* **1993**, *106*, 73−82.
(32) Afzal, M.; Yasmeen, G.; Saleem, M.; Afzal, J. *J. Therm. Anal. Calorim.* **2000**, *62*, 277−284.
(33) Hu, C. W.; Yao, J.; Yang, H. Q.; Chen, Y.; Tian, A. M. *J. Catal.* **1997**, *166*, 1−7.
(34) Chang, J.; Tsubaki, N.; Fujimoto, K. *Sekiyu Gakkaishi* **2000**, *43*, 357−360.
(35) Parlitz, B.; Schreier, E.; Zubowa, H, L.; Eckelt, R.; Lieske, E.; Lischke, G.; Fricke, R. *J. Catal.* **1995**, *155*, 1−11.
(36) Chen, L. D.; Wang, X. S.; Guo, X. W.; Guo, H. C.; Liu, H. O.; Chen, Y. Y. *Chem. Eng. Sci.* **2007**, *62*, 4469−4478.
(37) Han, J. X.; Sun, H.; Ding, Y. Q.; Lou, H.; Zheng, X. M. *Green Chem.* **2010**, *12*, 463−467.
(38) Ryymin, E. M.; Honkela, M. L.; Viljava, T. R.; Krause, A. *Appl. Catal., A* **2010**, *389*, 114−121.
(39) Ooi, T.; Asao, N.; Maruoka, K. *J. Synth. Org. Chem Jpn.* **1998**, *56*, 377−385.
(40) Kubicka, D.; Kaluza, L. *Appl. Catal., A* **2010**, *372*, 199−208.
(41) Idriss, H.; Diagne, C.; Hindermann, J. P.; Kiennemann, A.; Barteau, M. A. *J. Catal.* **1995**, *155*, 219−237.